Solution Properties of Polymer Mixtures

Michael S. Kent* and Matthew Tirrell

Department of Chemical Engineering and Materials Science, University of Minnesota, Minneapolis, Minnesota 55455

Timothy P. Lodge

Department of Chemistry, University of Minnesota, Minneapolis, Minnesota 55455

Received August 22, 1991; Revised Manuscript Received May 22, 1992

ABSTRACT: Polymer mixtures are investigated by studying the properties of a dilute probe polymer (polystyrene, PS) in the presence of a matrix polymer (poly(methyl methacrylate), PMMA) and a small molecule solvent. The solvent is chosen to be good for both polymers, and the concentration ranges are such that no phase separation occurs. Measurements include total intensity and dynamic light scattering, and viscometry. In the scattering experiments, a contrast-matching technique allows the study of the probe while in the presence of the matrix polymer. Specific points of interest are the effects due to the small positive interaction parameter χ between PS and PMMA and the importance of the ratio of probe and matrix molecular weights. In addition, the interpretation of changes in the initial dependence of the mutual diffusion coefficient on probe concentration, k_d(app), with matrix concentration is emphasized. By comparison of the data from ternary solutions with results for binary solutions it is found that χ has little or no effect on the cross Huggins coefficient or on the radius of gyration of the probe but does have a measurable influence on the mutual diffusion between the probe and the matrix. Comparison of the contraction of the radius of gyration of a probe ($M_P = 9.3 \times 10^5$) as a function of matrix concentration for three matrix polymers varying widely in molecular weight ($M_M = 1.3 \times 10^6, 7.0 \times 10^4, 7.0 \times 10^3$) gives insight into the molecular weight ratio for which the small matrix chains penetrate the domain of the larger probe coil in dilute solution. Apparently, there is little interpenetration between the probe and the 7.0×10^4 matrix polymer for $c_P^* < c_M < c_M^*$, whereas there is substantial interpenetration with the 7.0×10^3 matrix polymer over a similar range of matrix concentration; c_P^* (c_M^*) denotes the overlap concentration for the probe (matrix). The initial probe concentration dependence of the mutual diffusion coefficient between the probe and the matrix, k_d(app), has been determined as a function of matrix polymer concentration for three pairs of probe and matrix polymers ($9.3 \times 10^5/8.4 \times 10^5$, $2.3 \times 10^5/8.4 \times 10^5$, and $2.3 \times 10^5/6.6 \times 10^4$, respectively) and is interpreted in terms of the thermodynamic and frictional influence of the matrix polymer. The thermodynamic effect dominates at low concentrations of matrix polymer, and the frictional influence dominates at higher concentrations of matrix polymer. The thermodynamic effect, manifested by a decrease in the apparent second virial coefficient in the total intensity light-scattering experiment and a decrease in k_d(app) in the dynamic light-scattering experiment, appears to be the most significant effect of the matrix polymer in dilute solution.

Introduction

The study of the solution properties of polymer mixtures is valuable for several reasons. First, polymer blends are often processed while in solution and then concentrated by evaporation. Dissolving polymer mixtures in a common good solvent is one convenient way of mixing immiscible components. Depending on processing conditions, final structures and properties can be heavily influenced by the structures formed while in solution. Therefore, an understanding of how the solvent mediates interactions between unlike monomers is of great interest. Second, polymers are often synthesized in solution. The polymerizing mass is itself a polymer mixture containing both reactive growing chains and unreactive "dead" chains, along with small molecules such as solvent, unreacted monomer, inhibitors, and transfer agents. Understanding the influence of the unreactive dead polymers on the properties of the reactive growing chains is necessary in modeling the reaction kinetics. Third, studying polymer mixtures in solution has some advantages over melt studies in the characterization of the interaction between polymer molecules. In the diluted state, the effects of interactions between a relatively small number of coils can be studied. In addition, the time scale of solution measurements is usually much faster and the accuracy greater than measurements in solvent-free systems. The information obtained can then be a foundation upon which to approach the study of concentrated polymer mixtures or blends. For example, several solution studies[1-11] have focused on finding a convenient method for obtaining a value for the Flory–Huggins interaction parameter between different monomer types, which can then be used to predict the phase diagram for concentrated polymer mixtures or blends. While there are advantages to studying interactions between polymers in solution, it should be noted that excluded volume and hydrodynamic interactions provide some additional complications.

The goal of this work is to gain a greater understanding of fundamental interactions in solution between dissimilar polymers. This is accomplished by studying the properties of a dilute probe polymer (polystyrene, PS) in a solution comprising a matrix polymer (poly(methyl methacrylate), PMMA) and a small molecule solvent. The range of matrix polymer concentration encompasses both dilute and semidilute regimes. The focus is on the effects of the polymer–polymer interaction parameter, χ_{PM}, (the subscripts P and M refer to probe and matrix polymers, respectively) and the ratio of probe and matrix molecular weights. The interaction between PS and PMMA is known to be unfavorable but somewhat weak ($\chi_{PM} \approx 0.02$–0.03).[1-4] The solvent is chosen to be good for both polymers, and no phase separation occurs in any of the solutions in this study. The data are analyzed in ways analogous to conventional dilute solution measurements, with the solution properties of the dilute probe polymer varying

* Present address: Division 1815, Sandia National Laboratories, Albuquerque, NM 87185.

0024-9297/92/2225-5383$03.00/0

Table I
Homopolymers Used in this Work

M_w	M_w/M_n	supplier
	Polystyrene	
930 000	1.10	Scientific Polymer Products
233 000	1.06	Pressure Chemical
	Poly(methyl methacrylate)	
1 300 000	1.06	Polymer Laboratories
840 000	1.12	Scientific Polymer Products
70 000	1.04	Polymer Laboratories
66 000	1.3	Dupont[a]
7 000	1.05	Polymer Laboratories

[a] Kindly provided by Dr. D. Soguh.

with the concentration of the background polymer. In this way, the effects of the presence of the matrix polymer in the environment of the probe can be compared to the effects of a small molecule solvent of varying quality. Comparisons of this type reveal effects which are specific to the polymeric nature of the binary psuedosolvent, and thus give insight into the nature of polymer–polymer interactions.

The measurement techniques employed are total intensity light scattering, dynamic light scattering, and viscometry. In the light-scattering experiments, the solvent is chosen to be isorefractive with the matrix polymer to allow the study of the probe polymer while in the presence of the matrix polymer. The total intensity light-scattering experiments describe the change in the average dimension and thermodynamic environment of the probe as a function of the concentration of the matrix polymer. An earlier paper[12] focused on some experimental difficulties in the total intensity experiment, and the effect of the unfavorable interaction between PS and PMMA for polymers of similar molecular weight. The present work focuses on the importance of the ratio of the molecular weight of the two polymers. The dynamic light-scattering experiments examine the mutual diffusion between the probe and the binary psuedosolvent as a function of the concentration of the matrix polymer. Here it is shown that the matrix polymer has both a thermodynamic and frictional influence and that these are competing effects on the mutual diffusion process. The viscometric study complements the light-scattering experiments, which probe microscopic details, with a probe of a macroscopic solution property. In these experiments, further evidence is obtained regarding changes in coil size and the nature of interactions between dissimilar polymer molecules.

Experimental Section

Samples and Solutions. The characteristics and sources of the polymers used in this study are listed in Table I. For the dynamic light-scattering and viscosity measurements, solutions were prepared in HPLC grade toluene (Fisher Scientific). For the total intensity light-scattering measurements, solutions were prepared in ethyl benzoate (Aldrich). The solvents were filtered several times with 0.45-μm filters prior to use. Solutions were filtered with either 0.45-μm filters, if the solutions contained polymers with molecular weights of 8.4×10^5 or greater, or 0.20-μm filters, if the solutions contained polymers with smaller molecular weights. Concentrations of all solutions were determined gravimetrically, assuming additivity of volumes. Scattering cells for the dynamic light-scattering experiments were fashioned from scratch-free 12-mm-o.d. pyrex tubing. The cells were cleaned by soaking in a mixture of chromic and sulfuric acid, rinsing and drying, and then rinsing with filtered toluene to remove dust. The cells were then capped with Teflon tape and dried.

In the dynamic light-scattering experiments, a range of matrix polymer concentration was achieved by successive dilution. Cells were mixed at least one full day before being analyzed, which was found to be sufficient for the relatively dilute solutions used. For each set of experiments, representative cells were repeatedly analyzed over longer time intervals to verify that the solutions had reached equilibrium.

There have been reports[13] of anomalous slow diffusive modes reported for some PMMA homopolymer samples dissolved in good solvents. In the present work, it was found that samples which displayed such a slow diffusive mode, also displayed a strong scattering signal and an easily detected correlation function in toluene, which is nearly index-matched with PMMA. Therefore, each PMMA sample used in this work was examined by dynamic light scattering in toluene prior to use. Only those samples which showed no significant correlation in the scattered intensity in toluene over the dynamical range from 1 to 10^4 μs were selected for use.

Measurements. The dynamic light-scattering measurements were performed on a system which combines a Malvern Model PCS-100 photogoniometer, a Lexel Model 95 argon ion laser operated at 488 nm, and a Langley-Ford Model 1096 digital correlator. This correlator has 80 real-time channels spaced linearly in time, of which 64 were used to determine the decay of the autocorrelation function. The last 16 channels were delayed by 1000 sample times in order to determine the baseline. A calculated baseline was also determined for each experiment as (total counts)^2/(total number of sample times measured), and the two baselines were routinely compared to test for contributions from dust. Only correlation functions for which the two baselines differed by less than 0.1% were retained. An ITT FW-130 photo-counting photomultiplier tube was used to detect the scattered photons. All dynamic light-scattering experiments were performed in the homodyne mode. Toluene was used as an index-matching fluid to minimize reflections from glass surfaces. For each solution, correlation functions were measured at five angles ranging from 40 to 120°. All dynamic light-scattering measurements were performed at 18.0 ± 0.1 °C.

The experimental correlation functions were prepared for analysis by subtracting the baseline, dividing by the baseline, taking the natural logarithm, and then dividing by 2 (corresponding to a homodyne experiment). The data in this form were then routinely fit to a second-order cumulants expression.[14-17] The diffusion coefficient was determined as the slope of the decay rate plotted versus q^2 for the five scattering angles.

Recently, analyses of the dynamic scattering from ternary polymer–polymer–solvent solutions have been presented.[18,19] An important implication of these analyses is that under certain conditions, two modes may be observed in the scattering experiment even when one polymer is isorefractive with the solvent. The amplitude of the faster mode is predicted to be enhanced when the relative concentration of visible polymer is high. However, at high total polymer concentrations the amplitude of the faster mode is expected to be low. At low total polymer concentrations, the difference between the two decay rates becomes small. Therefore, two modes are only observed in an intermediate range of total polymer concentration, when the relative concentration of the visible polymer is high.

For the present work the conditions were such that only one mode, apparently the slower mode, was dominant. However, while the concentration of the probe was low, a range of probe concentrations was used since one goal of this work is to examine the initial dependence of the mutual diffusion coefficient on the concentration of the probe. Thus it is possible that the fast mode may be present to some extent in certain regions of the molecular weight–concentration space explored in this study. The sample time of the correlator was set to characterize only the slower mode, however, and so a faster mode would only be detected if it occurred on a time scale similar to that of the slower mode. To verify the presence of only one dominant relaxation mode, several data sets from each polymer–polymer–solvent combination were analyzed with Provencher's CONTIN[20] algorithm. The data sets were chosen to cover the entire range of matrix polymer concentrations for the higher concentration of probe polymer. In most cases, the amplitude of the dominant mode was greater than 85% of the scattering signal which is near the limit of the resolution capabilities of the CONTIN algorithm. The decay rates from the dominant mode agreed well with the results from

the cumulants analysis. In all cases the quality factors obtained from cumulants analysis in the ternary solution experiments were in the same range as those obtained when no matrix polymer was present. Plots of decay rate versus q^2 were linear for all cases, except for the few described below in which a slight upward curvature may be present. According to the above theory,[18,19] the presence of two modes should lead to curvature in the plot of decay rate versus q^2.

Whereas analysis of the correlation functions with the CONTIN algorithm has shown that the correlation functions are predominantly unimodal at higher concentrations of matrix polymer, and also when no matrix polymer is present, the CONTIN program does tend to yield several spurious modes for matrix polymer concentrations between zero and roughly $0.5c_M^*$, where c_M^* is the overlap concentration of the matrix polymer. The spurious modes probably arise because the sample time of the correlator was set to determine the correlation time of the slower (dominant) mode only, and thus a sufficient dynamical range was not examined to resolve a faster mode, if present. Unfortunately, the magnitude of the contribution of the faster mode for these cases cannot be precisely determined due to the limited dynamical range of the present data. However, the magnitude of any perturbations on the measured diffusion coefficients are small compared to the effects which are described in the following section, and the data for which there may be some question can be discarded without altering any of the conclusions of this work.

A Wyatt Dawn-F total intensity light-scattering instrument was used to measure the probe radius of gyration, R_g, molecular weight, M_w, and apparent second virial coefficient, A_2(app), as a function of matrix polymer concentration. Details of the apparatus, procedures, and data analysis were presented elsewhere.[12] Measurements were performed at 15 ± 1 °C, which has been shown[12] to be the temperature at which the refractive index increment for PMMA in ethyl benzoate vanishes for the wavelength of the present experiments (633 nm); the refractive index increment for PMMA in toluene at 633 nm, though small, is *not* zero anywhere near room temperature.

The viscosity measurements were made with a conventional Ubbelohde capillary viscometer from Schott-Gerate. The instrument determines elution times automatically. For each solution, a 15-mL sample was loaded into the viscometer, which was then placed into a thermostated bath. Measurements were initiated after approximately 5–10-min equilibration time, and were continued until several elution time readings agreed to within 0.5%. The capillary sizes were selected so that kinetic energy corrections were minimal. The elution times (t) were determined from an average of several readings and the kinematic viscosity (ν) calculated as $\nu = K(t - \theta)$, where K is the calibration constant of the viscometer and θ is the kinetic energy correction.[21,22] The viscosity η follows from $\eta = \nu\rho$, were ρ is the density of the solution. Since relatively dilute solutions were studied, the density of the solvent (toluene) was used in place of the density of the solution. The viscosity measurements were performed at 18.0 ± 0.1 °C.

Results and Discussion

The following section is divided into three parts, corresponding to the three experimental techniques: total intensity light scattering from isorefractive ternary solutions, viscometry, and dynamic light scattering from isorefractive ternary solutions.

Total Intensity Light Scattering from Isorefractive Ternary Solutions. In an earlier paper,[12] we discussed two experimental considerations that, if not handled correctly, could lead to substantial errors in experiments of this type. These involve a small mismatch in refractive index between the matrix polymer and solvent, and the range of the probe concentration employed. It was shown that with the system PS–PMMA–ethyl benzoate these difficulties can be eliminated, and results were given for one pair of probe and matrix polymers with similar molecular weights. The data were compared with small-angle neutron-scattering results for binary solutions, leading to the conclusion that the small positive interaction parameter χ_{PM} between PS and PMMA in the ternary solution has little or no effect on the contraction of the probe.

In the present work, the significance of the ratio of the probe and matrix molecular weights is examined. The apparent second virial coefficient and radius of gyration for a PS probe are reported as a function of matrix concentration for three PMMA matrix polymers differing widely in molecular weight. The polymers are all monodisperse standards. The molecular weight of the PS probe is 9.3×10^5, and the molecular weights of the PMMA matrix polymers are 1.3×10^6, 7.0×10^4, and 7.0×10^3. For each measurement of R_g and A_2(app), four solutions with c_P ranging up to 0.00125 g/mL, or $\sim 0.2c_P$, were prepared in ethyl benzoate. This range of PS concentration was shown previously[12] to be low enough to allow linear extrapolations to infinite dilution. The concentration of matrix polymer was the same in each of the four solutions.

Scaling predictions for $R_g(c)$ have been worked out in detail for both binary[23,24] and ternary solutions,[25–30] and have been reviewed elsewhere.[12,14] In terms of the ratio of probe and matrix molecular weights, two cases have been considered which have relevance in the present work. When the molecular weights of the probe and matrix polymers are similar (and effects due to χ_{PM} are negligible), the properties of the probe are described by the analysis for binary solutions. In this picture, there is very little interpenetration of the coils until the concentration reaches the overlap concentration c^*, at which point the coils begin to contract. This has been shown[12] to be the case for the PS (9.3×10^5)–PMMA (1.3×10^6)–ethyl benzoate system, where the probe begins to contract when $c_M \cong c_M^* \cong c_P^*$ and contraction of the probe for $c_M > c_M^* \cong c_P^*$ is consistent with the $R_g \sim c^{-0.125}$ power law predicted for binary solutions. The symbols c_M^* and c_P^* denote the concentration of polymer segments within the coil domain of the matrix polymers and probe polymers, respectively, at infinite dilution. This case is illustrated in Figure 1a.

The second case is when $M_P \gg M_M$ such that the matrix polymer penetrates the coil domain of the probe freely at all concentrations. For $c_M < c_M^*$, the matrix polymer essentially acts as a viscous solvent for a renormalized probe chain whose subunits are determined by the radius of the matrix chains. The effective solvent quality for the probe decreases with increasing c_M, but this effect is expected to be weak compared to the screening of excluded volume for $c_M > c_M^*$. This case is illustrated in Figure 1b. For $c_M > c_M^*$, the size of the renormalized subunits is determined by the correlation length of the matrix, and thus varies with c_M. The concentration dependence of the screening effect in semidilute solution is expected to be stronger than that for $c_M < c_M^*$.

The ratio of molecular weights for which the latter case is expected, i.e., where the matrix polymer begins to penetrate the domain of the probe freely, is as yet unknown. The highest and lowest molecular weight matrix polymers in this study were chosen to correspond to the two extreme cases described above. The third matrix polymer lies in between the two extremes and may give some insight into the ratio of molecular weights for which the matrix polymer can penetrate the domain of the probe freely.

There have been several experimental studies of this type reported in the literature;[5,9,30–37] however, there is considerable conflict among the results of these studies. Two studies which covered a significant range of c_M for various ratios of M_P/M_M each suggest a different scaling

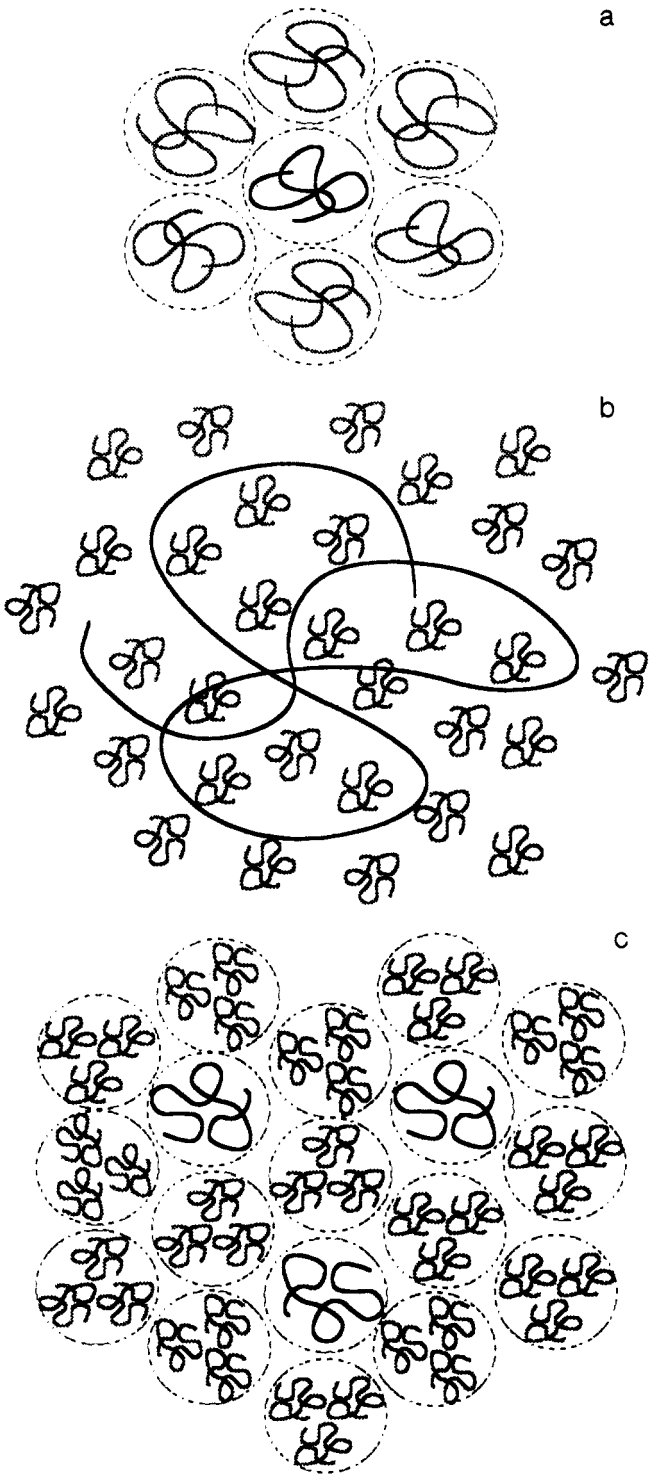

Figure 1. (a) Ternary solution where $M_P \cong M_M$ and effects due to χ_{PM} are negligible. The probe polymer is indicated by the dark lines. At $c/c^* = 1$, the coils begin to contract. (b) Ternary solution where $M_P \gg M_M$ and effects due to χ_{PM} are negligible. The small polymer penetrates the domain of the probe freely and acts as a viscous solvent. Screening of excluded volume in the probe chain is expected to be weak for $c_M < c_M^*$. (c) Ternary solution where $M_P > M_M$, $c_P^* < c_M < c_M^*$, and effects due to χ_{PM} are negligible. If the small chains are largely excluded from the domain of the probe, the probe should begin to contract when $c_M \cong c_P^*$, where the density of segments outside the domain of the probe coil is comparable to the density of segments inside the domain of the probe coil.

of c_M in order to obtain a universal curve for the decrease in R_g/R_{go}. When the data for both studies are plotted[14] versus c_M, first as c_M/c_M^* and then as c_M/c_P^*, the difference is clearly seen; R_g/R_{go} of ref 34 scales approximately with c_P^* while the data of ref 33 scale more clearly with c_M^*. The disagreement may be due at least in part to the experimental difficulties described in the previous paper.[12]

In Table II, M_w, A_2(app), and R_g of the probe are given as a function of c_M for all three matrix polymers. In Figure 2a, the measured M_w of the probe is plotted versus c_M for the three PMMA matrix polymers. The measured molecular weight of the probe is constant within experimental error over the entire range of matrix polymer concentration, indicating that the refractive index match between PMMA and ethyl benzoate is sufficiently precise. A_2(app) and R_g of the probe are plotted versus c_M for the three PMMA matrix polymers in Figure 2b,c, respectively, and versus c_M/c_M^* in Figure 3a,b. The arrows on Figure 2b,c indicate the c_M^* values, which have been estimated as $1.5/[\eta]$, where the expression[38] $[\eta] = 0.0055M^{0.76}$ for PMMA in benzene at 20 °C was used to estimate the intrinsic viscosity.

Whereas the apparent second virial coefficients seem to scale with c_M^*, the decrease of the radius of gyration clearly does not scale with c_M^*. From Figure 2c, the decrease in the radius of the probe with c_M is nearly the same in the 7.0×10^4 PMMA matrix polymer as in the 1.3×10^6 PMMA matrix polymer. Furthermore, the smaller difference in matrix molecular weight between 7.0×10^4 and 7.0×10^3 results in a very significant difference in the contraction of the probe. This is shown more clearly in Figure 4, which displays the radius of gyration versus c_M on a linear scale.

As described in an earlier paper, the data involving the highest molecular weight matrix polymer seem to be consistent with the scaling predictions. The probe begins to contract at $c_M \cong c_M^* \cong c_P^*$. The decrease in the radius of the probe observed for $c_M > c_P^*$ is consistent with the predicted relation $R_g \sim c_M^{-0.125}$, although the concentration range is rather limited and the subset of data chosen to be included in the fit is somewhat arbitrary. The data for the lowest molecular weight matrix polymer also appear to be in accord with the scaling picture. Here, screening of excluded volume is expected to be weak for $c_M < c_M^*$. All the experiments fell in the range $c_M < c_M^*$ for the 7.0×10^3 matrix polymer, and the radius of gyration of the probe indeed shows a much weaker dependence on matrix polymer concentration than for the experiments involving the highest molecular weight matrix polymer. In fact, the radius of the probe seems to level off at a matrix polymer concentration of 0.10 g/mL.

Flory[39] originally predicted that when $N_M < N_P^{1/2}$, where N_M and N_P are the degree of polymerization of the matrix and probe polymers, respectively, the radius of the probe would be expanded in the melt, but the expansion would be reduced from that occurring in a good solvent by $N_M^{-1/5}$. This may be viewed as a renormalization of the excluded volume in the probe chain due to the presence of the short chains. The values of N_P and N_M in the present work are ~9000 and 70, and so $N_M < N_P^{1/2}$ holds and the fact that R_g levels off at a value greater than the θ dimension (Figure 4) is consistent with Flory's prediction. The expansion of a long chain in a melt of short chains has been observed previously by neutron scattering.[40]

The data for the 7.0×10^4 PMMA matrix polymer, however, do not seem to be consistent with the scaling picture. The concentration range is such that data are obtained for c_M both below and above c_M^*. Since $M_P > M_M$ for this pair, the scaling picture is as depicted in Figure 1b, and the screening of excluded volume is expected to be weak below c_M^*. However, in Figure 2c, the data show a contraction of the probe for $c_M < c_M^*$ that depends as strongly on c_M as the contraction of the probe in the

Table II
Total Intensity Light-Scattering Results for Polystyrene (M_w = 930 000) in the Presence of Poly(methyl methacrylate) Matrix Polymers in Ethyl Benzoate at 15 °C

poly(methyl methacrylate) concn × 10^2 (g/mL)	apparent mol wt × 10^{-5}	apparent second virial coeff ((mL mol)/g^2)	radius of gyration (Å)
Matrix Polymer: Poly(methyl methacrylate) M_w = 1 300 000			
0.000	9.21	2.06×10^{-4}	372
0.000	9.40	1.78×10^{-4}	388
0.000	9.92	1.82×10^{-4}	403
0.000	10.4	2.00×10^{-4}	405
0.0534	9.67	1.67×10^{-4}	399
0.0898	8.72	8.45×10^{-5}	383
0.116	10.0	1.26×10^{-4}	394
0.162	9.77	1.35×10^{-4}	382
0.177	9.50	1.40×10^{-4}	403
0.200	9.78	8.32×10^{-5}	388
0.264	9.80	8.39×10^{-5}	376
0.264	9.83	7.03×10^{-5}	385
0.264	9.49	7.72×10^{-5}	398
0.350	9.53	7.37×10^{-5}	376
0.499	9.73	3.04×10^{-5}	386
0.600	8.87	1.96×10^{-5}	375
0.738	10.1	4.07×10^{-5}	371
0.738	9.21	8.71×10^{-6}	390
0.740	9.73	8.99×10^{-6}	384
0.893	10.4	6.09×10^{-5}	377
1.05	9.75	1.22×10^{-5}	369
1.58	9.75	-1.45×10^{-5}	368
1.68	9.90	-9.98×10^{-6}	349
2.10	10.0	-7.02×10^{-6}	357
2.42	10.1	-1.47×10^{-5}	350
2.84	10.3	-5.02×10^{-6}	342
3.14	9.90	-3.20×10^{-5}	342
3.20	10.3	-7.61×10^{-6}	340
4.09	10.0	-1.55×10^{-5}	334
5.13	9.32	-1.11×10^{-5}	318
6.29	9.46	-8.91×10^{-5}	312
6.40	8.92	-5.85×10^{-5}	305
Matrix Polymer: Poly(methyl methacrylate) M_w = 70 000			
0.000	10.0	2.30×10^{-4}	404
0.000	9.69	2.10×10^{-4}	398
0.000	10.2	2.40×10^{-4}	400
0.000	10.4	2.49×10^{-4}	396
0.100	10.3	2.37×10^{-4}	392
0.200	9.32	1.95×10^{-4}	382
0.289	9.84	2.02×10^{-4}	394
0.380	9.71	2.01×10^{-4}	386
0.524	9.81	2.02×10^{-4}	385
0.703	9.29	1.61×10^{-4}	386
0.802	9.09	1.53×10^{-4}	378
1.11	9.55	1.67×10^{-4}	374
1.64	9.62	1.59×10^{-4}	375
2.10	9.38	1.29×10^{-4}	367
2.89	9.23	8.29×10^{-5}	364
2.92	9.46	1.01×10^{-4}	357
3.85	9.07	5.03×10^{-5}	348
4.82	9.20	4.11×10^{-5}	342
5.55	9.72	6.16×10^{-5}	328
5.77	9.15	2.20×10^{-5}	327
6.79	9.20	2.96×10^{-5}	323
11.5	9.94	-5.36×10^{-6}	296
14.7	10.5	-2.40×10^{-5}	271
Matrix Polymer: Poly(methyl methacrylate) M_w = 7000			
1.00	10.7	2.44×10^{-4}	401
2.00	10.3	2.22×10^{-4}	383
3.00	9.52	1.86×10^{-4}	378
4.50	9.81	1.83×10^{-4}	381
5.00	9.62	1.73×10^{-4}	375
6.20	9.75	1.64×10^{-4}	373
8.70	10.1	1.68×10^{-4}	357
10.4	9.95	1.50×10^{-4}	350
16.0	9.72	1.04×10^{-4}	353
20.5	9.78	8.07×10^{-5}	353

presence of the highest molecular weight matrix polymer, where $c_M > c_P^* \cong c_M^*$. In addition, no significant change

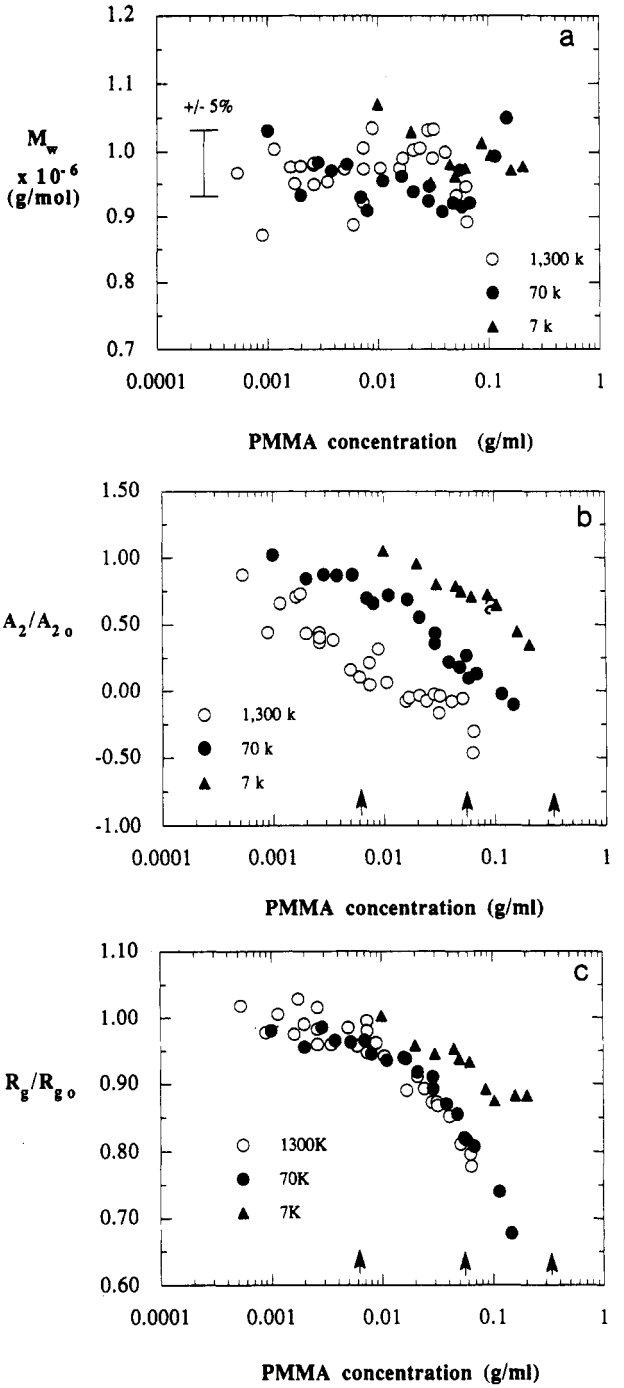

Figure 2. (a) Apparent M_w of the PS probe versus c_{PMMA} for three PMMA matrix polymers in ethyl benzoate at 15 °C. The numbers in the legend indicate the molecular weights of the matrix polymers. (b) Decrease in the apparent second virial coefficient of the PS probe with increasing matrix concentration for the three PMMA matrix polymers. The arrows indicate the c_M^* values. (c) Decrease in the radius of gyration of the PS probe with increasing matrix concentration for the three PMMA matrix polymers. The arrows indicate the c_M^* values.

occurs as the concentration passes through c_M^*. One possible explanation for the relatively strong decrease in the radius of the probe for $c_M < c_M^*$ in the presence of the 7.0×10^4 matrix polymer is that the matrix polymer does not penetrate the domain of the probe coil freely. Scaling approaches have treated only the limit of $M_P \gg M_M$. In that case, the matrix polymer is assumed to penetrate the domain of the probe coil freely. This must be true only when M_P is sufficiently larger than M_M, since interpenetration is very limited when $M_P \cong M_M$. The case of $M_P > M_M$, but no interpenetration, is illustrated in Figure 1c. In this picture,[37] since the matrix polymer is largely

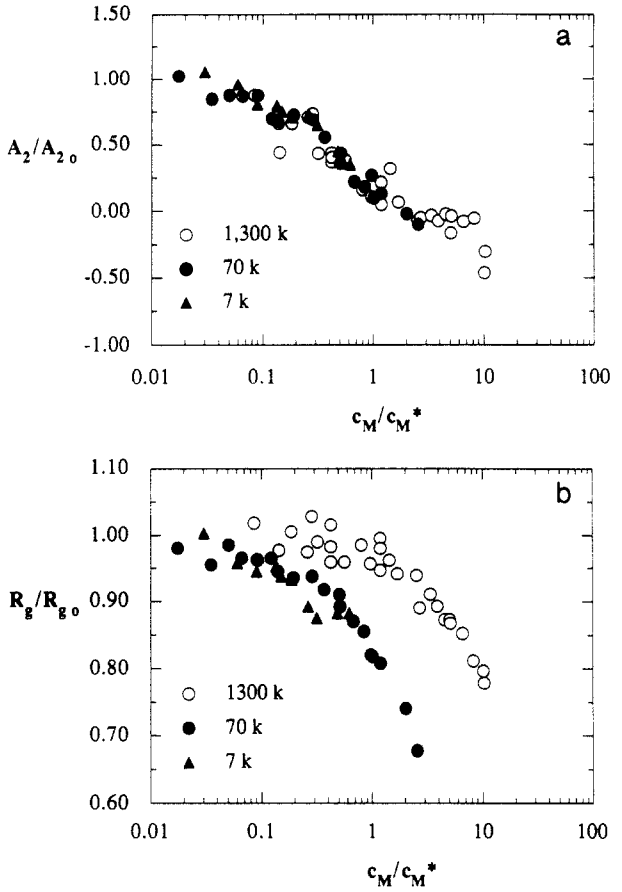

Figure 3. (a) Decrease in the apparent second virial coefficient of the PS probe with matrix concentration scaled with c_M^* for the three PMMA matrix polymers. (b) Decrease in the radius of gyration of the PS probe with matrix concentration scaled with c_M^* for the three PMMA matrix polymers.

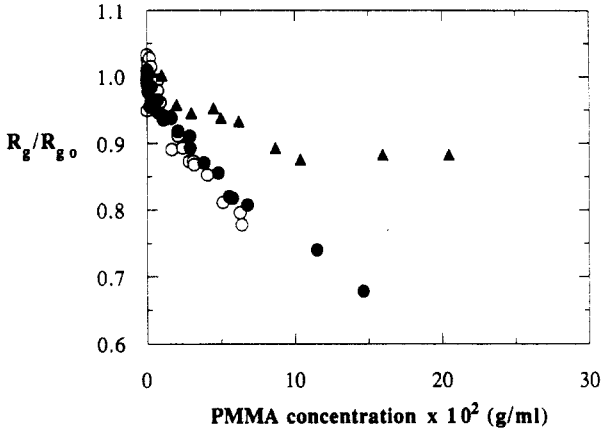

Figure 4. Decrease in the radius of gyration of the PS probe with increasing matrix concentration for the three PMMA matrix polymers. The symbols are the same as in the preceding plots.

excluded from the domain of the probe coil, contraction of the probe begins at $c_M = c_P^*$, where the concentration of polymer segments outside the probe coil (from matrix polymers) is equal to the concentration of segments inside the probe coil (from the probe polymer). Therefore, the concentration at which the probe begins to contract depends only on the molecular weight of the probe coil, and is largely independent of the molecular weight of the matrix polymer as long as the matrix polymer does not penetrate the domain of the probe coil freely. This would explain why the contraction of the probe is nearly the same in the 1.3×10^6 matrix polymer as in the 7.0×10^4 matrix polymer. The difference between the decrease in the radius of the probe with c_M in the presence of the 7.0×10^4 and 7.0×10^3 matrix polymers, then, arises because the former does not penetrate the coil domain of the probe, while the latter does.

This picture is also consistent with the behavior of the apparent second virial coefficient. For the highest molecular weight matrix polymer, the apparent second virial coefficient of the probe decreases to zero even before the radius of the probe begins to show noticeable contraction. This could be due to the fact that A_2(app) reflects the volume of solution excluded from the probe coil by the matrix coils, as well as the excluded volume between probe chains. The former is important if there is limited interpenetration between probe and matrix polymers. The apparent second virial coefficient derived from fluctuation theory[41] may be written as[12]

$$A_2(\text{app}) = A_P - \frac{A_{PM}^2 M_M c_M}{2(1 + 2A_M M_M c_M)} \qquad (1)$$

In the limit that the matrix polymer penetrates the domain of the probe coil freely, $A_{PM} = 0$ and the dependence of A_2(app) on c_M comes from the first term in eq 1; A_P would reflect the decrease in solvent quality for the probe as c_M increases. In the limit that the matrix polymer is excluded from the domain of the probe coil, the dependence of A_2(app) on matrix polymer concentration is due to the second term on the right hand side of eq 1. The fact that the data for A_2(app) in the presence of the 7.0×10^4 and 1.3×10^6 matrix polymers coincide when plotted versus c_M/c_M^* suggests that A_2(app) is largely reflecting the volume of solution occupied by the matrix coils, or the second term in eq 1, rather than the screening of excluded volume inside the probe coil, and thus that neither matrix polymer penetrates the domain of the probe coils to a significant degree.

Nose[29] has developed a scaling analysis for the apparent second virial coefficient, in addition to the radius of gyration. This calculation is based on the assumption that the decrease in A_2(app) arises from the screening of excluded volume inside the probe coil. Thus, a decrease in A_2(app) is predicted to correspond to a decrease in the radius of gyration. When $M_P = M_M$, no decrease in A_2(app) is expected until the overlap concentration is reached, where the radius of the probe begins to contract. The behavior of the probe in the presence of the highest molecular weight matrix polymer is not consistent with this prediction. Apparently, only the first term on the right-hand side of eq 1 has been considered in Nose's analysis.

In summary, it is clear that data of sufficient precision can be obtained to investigate the fundamental nature of polymer–polymer interactions through comparison of the decrease in the apparent second virial coefficient and radius of gyration of the probe with matrix polymer concentration. If the above interpretation of the contraction of the probe in the presence of the 7.0×10^4 matrix polymer is correct, the fact that there is very little penetration of this polymer into the coil domain of the probe is somewhat surprising, since the ratio of the probe and matrix molecular weights is roughly a factor of 14. Furthermore, somewhere between 7.0×10^4 and 7.0×10^3 there appears to be a crossover from noninterpenetration to free interpenetration with the probe. The transition between the two limits of noninterpenetrating ($M_P = M_M$, $c < c^*$) and interpenetrating ($M_P \gg M_M$, $c_M < c_M^*$) may be more accurately characterized by a fairly abrupt transition occurring over a limited range of M_P/M_M than by a continuous transition with increasing M_P/M_M. More experiments would be required to characterize the inter-

action of probe and matrix polymers with different molecular weights in detail. If the same experiment is performed with other matrix polymers, the above interpretation predicts that all the curves of R_g/R_{go} versus c_M should superpose unless the matrix polymer is small enough to penetrate the coil domain of the probe. Nevertheless, the present results give some insight into the molecular weight ratio for which a smaller polymer penetrates the domain of the larger coil and thus at which the smaller coil can be viewed as an effective solvent for the larger polymer, affecting the larger polymer only by altering the viscosity and quality of the solvent.

Viscometry. The viscosity increment of a PS probe polymer (9.3×10^5) was determined as a function of the concentration of a PMMA matrix polymer (8.4×10^5). Four concentrations of probe polymer were used for each determination of the viscosity increment. The concentration of matrix polymer was the same in each of the four solutions and the matrix polymer and small molecule solvent were treated as a psuedosolvent. The data were plotted in the same manner as for conventional dilute solution intrinsic viscosity determinations, except that the solvent viscosity was replaced by the viscosity of the psuedosolvent. As shown below, the intercept of the viscosity increment plot for the ternary solution may be expressed as a function of the intrinsic viscosities and Huggins coefficients, which can be examined as a function of matrix polymer concentration to study the effects of interactions between unlike polymers. One important result from this study is the value of the cross Huggins coefficient, $k_{H,PM}$.

The slope of the viscosity increment plots will be referred to as the apparent intrinsic viscosity $[\eta](app)$. This quantity has been determined for both binary and ternary solutions as a function of matrix polymer concentration. The viscosity of binary solutions at low concentrations may be expressed as

$$\eta(c) = \eta_s(1 + [\eta]c + k_H[\eta]^2c^2 + ...) \quad (2)$$

where η_s is the solvent viscosity, $[\eta]$ is the intrinsic viscosity, and k_H is the Huggins coefficient. The viscosity of ternary solutions at low concentrations may similarly be expressed as

$$\eta(c_P,c_M) = \eta_s(1 + [\eta]_P c_P + [\eta]_M c_M + k_{H,P}[\eta]_P{}^2 c_P{}^2 + k_{H,M}[\eta]_M{}^2 c_M{}^2 + 2k_{H,PM}[\eta]_P[\eta]_M c_P c_M ...) \quad (3)$$

The apparent intrinsic viscosity, $[\eta](app)$, due to one polymer in a ternary solution, is determined experimentally as

$$[\eta](app) = \left.\frac{\eta(c_2) - \eta(c_1)}{\Delta c \eta(c_1)}\right|_{\Delta c \to 0} \quad (4)$$

where $c_2 = c_1 + \Delta c$, c_1, which represents the "matrix" polymer concentration, is fixed, and Δc is the "probe" polymer concentration.

Substituting eq 2 into eq 4 gives

$$[\eta](app) = \frac{\eta_s}{\eta(c_1)}([\eta] + k_H[\eta]^2 2c_1 + k_H[\eta]^2\Delta c)|_{\Delta c \to 0} \quad (5)$$

Therefore, for a plot of $[\eta(c_2) - \eta(c_1)]/\Delta c\eta(c_1)$ vs Δc, for small Δc, the intercept is

$$[\eta](app) = \frac{\eta_s}{\eta(c_1)}([\eta] + 2k_H[\eta]^2 c_1) \quad (6)$$

Note that when $c_1 = 0$, $[\eta](app) = [\eta]$.

In the ternary solution experiment, the measured quantity is

$$[\eta](app) = \left.\frac{\eta(c_P,c_M) - \eta(0,c_M)}{c_P\eta(0,c_M)}\right|_{c_P \to 0} = \frac{\eta_s}{\eta(0,c_M)}([\eta]_P + k_{H,P}[\eta]_P{}^2 c_P + 2k_{H,PM}[\eta]_P[\eta]_M c_M)|_{c_P \to 0} \quad (7)$$

Therefore, for a plot of $[\eta(c_P,c_M) - \eta(0,c_M)]/c_P\eta(0,c_M)$ vs c_P, for small c_P, the intercept is

$$[\eta](app) = \frac{\eta_s}{\eta(0,c_M)}([\eta]_P + 2k_{H,PM}[\eta]_P[\eta]_M c_M) \quad (8)$$

From eqs 6 and 8, plots of $[\eta](app)\eta(0,c_M)/\eta_s$ vs c_M should be linear, with slopes related to Huggins coefficients.

Results from binary and ternary solutions were compared to determine if the interaction between unlike monomers produces any additional effects. Two features were examined: the dimension of the probe coils as evidenced by $[\eta]_P$ and the interaction between probe and matrix polymers as evidenced by $k_{H,PM}$. The intrinsic viscosity is a well-accepted measure of the coil dimension in binary solutions, with $[\eta] \sim R^3$. While the intrinsic viscosity is defined in the limit of infinite dilution, the parameters $[\eta]_P \sim R_P{}^3$ and $[\eta]_M \sim R_M{}^3$ were used in the ternary solution expressions as measures of coil size. If the probe coils contract due to the presence of the matrix polymer, $[\eta]_P$ should decrease with the concentration of matrix polymer. From eq 8, this should lead to downward curvature in a plot of $[\eta](app)\eta(0,c_M)/\eta_s$ vs c_M. If the nature of binary interactions are different when the two polymers are of different types, the difference should be evidenced in a comparison of $k_{H,P}$, $k_{H,M}$, and $k_{H,PM}$.

The intrinsic viscosities and Huggins coefficients for PS and PMMA in toluene were each determined from the dilute, binary solution data. The values for the PS probe are 215 mL/g and 0.33, respectively. The corresponding values for the PMMA matrix polymer are 126 mL/g and 0.41, respectively. For concentrations below 0.010 g/mL, the measured viscosities for both PS and PMMA in toluene agree well with values calculated according to eq 2 using these parameters.[14]

The ternary solution viscosities were plotted according to eq 7, and the resulting intercepts ($[\eta](app)$) are given in Table II. In order to determine analogous quantities for binary solutions of PS and PMMA in toluene according to eq 4, polynomials were fit to binary solution viscosity data and used for interpolation. The resulting intercepts for various "matrix" concentrations of the binary solutions are also given in Table III. Note that although the apparent intrinsic viscosity decreases with matrix polymer concentration, this is not necessarily an indication of coil contraction.

The $[\eta](app)$ values multiplied by $\eta(c_M)/\eta_s$ for binary solutions of PS and PMMA in toluene and for ternary solutions of PS and PMMA in toluene are plotted versus matrix polymer concentration in Figure 5a–c. For the binary solutions, the data for concentrations below 0.010 g/mL are reasonably linear and agree well with the corresponding values calculated from eq 6 using the measured values of $[\eta]$ and k_H, indicating that eq 2 is an adequate representation of the viscosity for concentrations below 0.010 g/mL and that the parameters $[\eta]$ and k_H are not dependent on concentration over the measured range.

For the ternary system, the corresponding plot in Figure 5c is also linear for concentrations below 0.010 g/mL and

Table III
Results from Viscosity Increment Plots

matrix polymer concn × 10^2 (g/mL)	intercept [η] (app) (mL/g)	matrix polymer concn × 10^2 (g/mL)	intercept [η] (app) (mL/g)
Polystyrene in Toluene			
0.000	215	0.867	124
0.217	182	1.08	114
0.433	157	1.30	106
0.650	138		
Poly(methyl methacrylate) in Toluene			
0.000	126	0.867	92.4
0.217	119	1.08	84.9
0.433	110	1.30	78.3
0.650	101		
Polystyrene in Binary Solvent (Poly(methyl methacrylate) + Toluene)			
0.178	199	0.781	153
0.347	181	1.09	129
0.555	160	1.28	131

the value of $k_{H,PM}$, 0.34, determined from the slope is similar to the values for the two binary solutions. The fact that the plot of $[\eta](\text{app})\eta(0,c_M)/\eta_s$ vs c_M for the ternary system has the same features as the plots for the binary solutions strongly suggests that there are no additional effects occurring in the ternary solutions. There is no evidence of the downward curvature that would result if the probe were contracting in the presence of the matrix polymer. For example, if R_g for the PS probe at 0.010 g/mL PMMA were 20% smaller than its dilute solution value, the ordinate value would be $0.80^3 = 0.51$ times the value on the curve in Figure 5c. The similarity of the coefficients $k_{H,P}$, $k_{H,M}$, and $k_{H,PM}$ also implies that the interaction between unlike polymers is not significantly different than the interactions between identical polymers.

For concentrations below 0.010 g/mL, the ternary solution viscosities calculated from eq 3, with $[\eta]_P$ = 215 mL/g, $[\eta]_M$ = 126 mL/g, $k_{H,P}$ = 0.33, $k_{H,M}$ = 0.41, and $k_{H,PM}$ = 0.34, agree very well with the experimental values.[14] This is further indication that eq 3 is an adequate representation of the data for concentrations below 0.010 g/mL and that there is no need to invoke coil contraction to describe the viscosity data. This is completely consistent with the direct measurements of R_g by light scattering, which show no contraction in this concentration range (Figure 2c). The upward curvature in Figure 5a for concentrations higher than 0.010 g/mL indicates that higher order terms are needed to describe the viscosity in that region. Higher order terms are more important for the binary PS–toluene solution than for the solutions containing PMMA because toluene is a much better solvent for PS than for PMMA.[42]

A similar study of the viscosity of polymer–polymer–solvent ternary solutions has been reported by Moszkowicz and Rosen.[43] The ternary system in their study was polystyrene–polybutadiene–toluene, and the polymers were polydisperse and of lower molecular weight than in the present study. While they concluded that there were no qualitative differences observed when either polybutadiene or PS were used as the matrix polymer, similar to the results of the present study of PS and PMMA, they claimed that the decrease in the apparent intrinsic viscosity with matrix polymer concentration supported the hypothesis that the PS probe coils were contracting. That is contrary to the conclusions of this study, in which the results are interpreted as strong evidence that no coil contraction takes place at low concentrations. The apparent intrinsic viscosity does not directly reflect the size of the probe as does the intrinsic viscosity, but only does so indirectly through the parameters in eq 6 and 8. Finally, it should be noted that the use of eqs 2 and 3 to represent the viscosity has limited the scope of this study to effects which occur at concentrations below 0.01 g/mL.

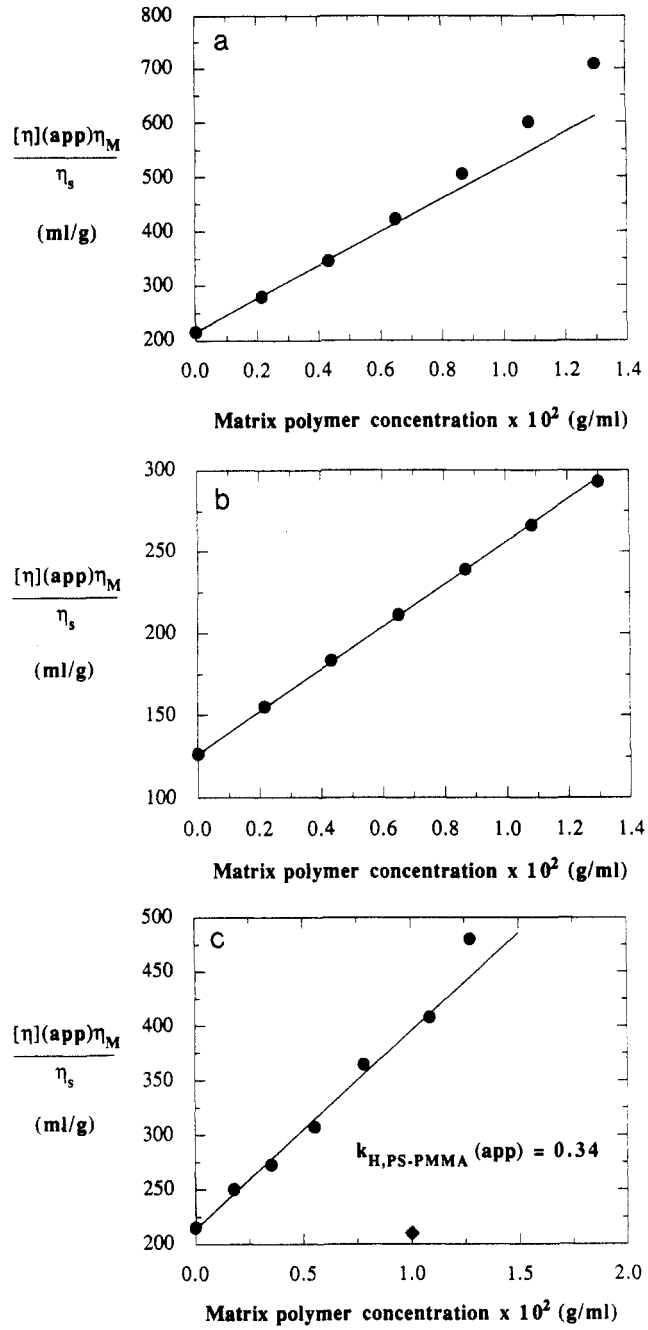

Figure 5. (a) Viscosity data for PS in toluene plotted according to eq 6. $[\eta](\text{app})$ is the intercept of the viscosity increment plots. (b) Viscosity data for PMMA in toluene plotted according to eq 6. (c) Viscosity data for the ternary system PS–PMMA–toluene plotted according to eq 8. The solid diamond represents the expected value if the probe radius had decreased 20% at 0.01 g/mL PMMA.

Dynamic Light Scattering from Isorefractive Ternary Solutions. The diffusion coefficient measured in this experiment requires careful definition. Although the solution is a ternary solution containing two polymers and a solvent, only fluctuations in the concentration of the probe are detected. Thus, the diffusion coefficient should be viewed as describing the rate of mutual diffusion between the probe and the binary solvent composed of the matrix polymer and the small molecule solvent. The following expression for the mutual diffusion coefficient (derived in the Appendix) is due to the work of Hanley:[44]

$$D_{PP} = D_0 \frac{\hat{H}(c_P,c_M)}{\hat{f}(c_P,c_M)} \tag{9}$$

where $\hat{H}(c_P,c_M)$ and $\hat{f}(c_P,c_M)$ are dimensionless thermodynamic and frictional functions, respectively, and $D_0 = k_BT/f_0$ is the value of D_{PP} at infinite dilution of the probe when $c_M = 0$, where k_B is Boltzmann's constant, T is the temperature, and f_0 is the friction felt by an isolated probe coil due to the solvent. It is shown in the Appendix that $\hat{H}(c_P,c_M)$ can be obtained from total intensity light scattering. The friction function $\hat{f}(c_P,c_M)$ may also be obtained independently, from forced Rayleigh scattering, for example.

The dynamic light-scattering experiments were designed to determine the initial dependence of D_{PP} on the concentration of the probe, as a function of the concentration of matrix polymer. In binary solutions, the initial concentration dependence of the mutual diffusion coefficient is given by

$$D = \frac{k_BT}{f_0}(1 + k_dc + ...) \tag{10}$$

where

$$k_d = 2A_PM_P - k_f + V_P \tag{11}$$

k_f is the linear term in the concentration expansion for the friction coefficient, and V_P is the partial specific volume of the polymer. The coefficient k_d is thus given by a term coming from the thermodynamic driving force, $2A_PM_P$, and an opposing term coming from the frictional resistance, k_f; the third term, V_P, is small. Previous work[45-50] has shown that the value of k_d is large and positive for high molecular weight polymers in good solvents, where the term involving A_2 dominates, while in θ solvents ($A_2 = 0$) k_d has a small negative value which reflects k_f. In ternary solutions, the coefficient of the corresponding linear term describing the initial dependence of the mutual diffusion coefficient on probe concentration is determined experimentally as

$$k_d(\text{app}) = \left.\frac{\partial D_{PP}/D_0}{\partial c_P}\right|_{c_P=c_P^A} \tag{12}$$

where $\bar{c}_P^A$ is the mean of the range of probe concentration used to determine the initial slope. Thus

$$k_d(\text{app}) = \left.\frac{\partial \hat{H}(c_P,c_M)}{\partial c_P}\right|_{\bar{c}_P^A,c_M} - \left.\frac{\hat{H}(c_P,c_M)\dfrac{\partial \hat{f}(c_P,c_M)}{\partial c_P}}{\hat{f}(c_P,c_M)^2}\right|_{\bar{c}_P^A,c_M} \tag{13}$$

Using this expression, independent measurements of the thermodynamic and frictional functions, or theoretical expressions for those functions, may be directly compared with the results of the dynamic light-scattering experiments.

In this section, results are presented for k_d(app) as a function of c_M. Initially, experimental values of k_d(app) as a function of c_M for three pairs of probe and matrix polymers will be compared to estimates of k_d(app) calculated from eq 13 using thermodynamic and frictional functions obtained from experimental data, in order to establish that eq 13 gives an adequate description of k_d(app). A discussion of a theoretical expression for k_d(app) involving only lowest order terms will then be presented to obtain a better physical understanding of the features observed in the experimental data.

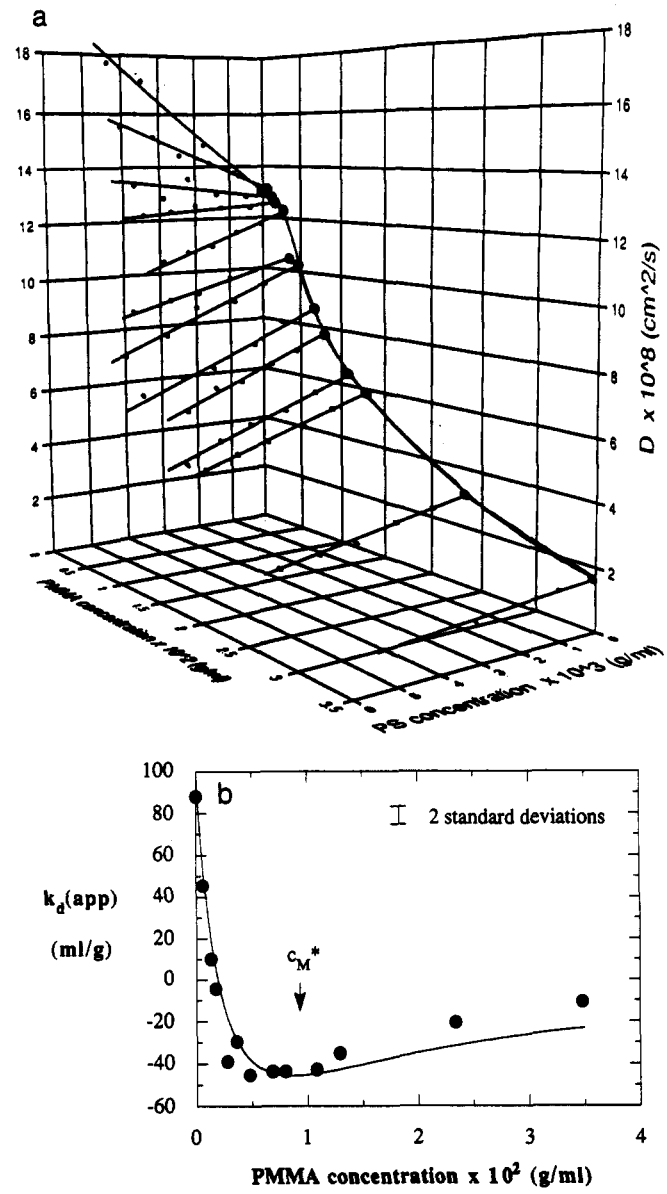

Figure 6. (a) Mutual diffusion coefficient D_{PP} as a function of the concentration of both probe and matrix polymers. The large circles represent the diffusion coefficients extrapolated to infinite dilution in the probe. The solid curve through the large circles thus represents the decrease in the tracer diffusion coefficient with matrix polymer concentration. The solid lines represent the initial dependence on the concentration of the probe, which involves both the thermodynamic and frictional influence of the matrix polymer. (b) k_d(app) versus matrix polymer concentration for the data in (a). The k_d(app) values are determined as the slope divided by the constant $D_{PP}(c_P \to 0, 0)$. c_M^* was calculated as $1.5/[\eta]$, with $[\eta] = 0.0055M^{0.76}$. The solid curve was calculated from eq 13 using experimental estimates of the thermodynamic and friction functions. The error bar indicates the statistical uncertainty in the experimental k_d(app) values.

To determine the initial dependence of D_{pp} on c_P as a function of c_M, five solutions were prepared for each c_M, where c_P was incremented in each solution. All five probe concentrations were in the dilute regime. Results for one pair of probe and matrix polymers are given in Figure 6a, where the D_{PP} is plotted as a function of the concentrations of both the PS probe ($M_P = 9.3 \times 10^5$) and the PMMA matrix ($M_M = 8.4 \times 10^5$) polymers. The large circles represent the diffusion coefficient extrapolated to infinite dilution in probe concentration, or the tracer diffusion coefficient. The tracer diffusion coefficient in this case is

given by

$$D_{TR}(c_M) = D_{PP}(c_P \to 0, c_M) = \frac{k_B T}{f(0,c_M)} \quad (14)$$

and represents the purely frictional influence of the matrix polymer. Most previous experiments involving dynamic light scattering from isorefractive ternary solutions have focused on the comparison of these values with theories for self-diffusion in concentrated polymer systems, such as the reptation theory.[51] This work focuses on the slopes of the lines in Figure 6a, which represent the initial dependence of D_{PP} on c_P, and which involve both the thermodynamic and frictional influences of the matrix polymer.

With no matrix polymer present, the slope is large and positive, due to the large second virial coefficient according to eq 10; i.e., toluene is a good solvent for polystyrene. As c_M increases, there is a rapid decrease in the slope. The slope becomes negative and reaches a minimum at roughly c^* of the matrix polymer and then begins to increase and approaches zero at higher concentrations of matrix polymer. This is shown more clearly in Figure 6b, in which the slope divided by D_0, or k_d(app), is plotted versus matrix polymer concentration. The goal of this work is to understand the behavior of k_d(app) versus c_M and to determine the role of the polymer–polymer interaction parameter in affecting the rate of dissipation of fluctuations in the concentration of the probe.

The thermodynamic function in eq 9 was measured[14] for this system by total intensity light scattering. Second-order polynomials were fit to $Kc_P/R_{\theta=0}$ versus c_P as a function of c_M, over the same range of c_P and c_M as in the dynamic experiments. Measurement of the frictional function by forced Rayleigh scattering requires the synthesis of a dye-labeled polystyrene probe of the same molecular weight as used in the dynamic light-scattering experiments. This is currently in progress, but for the present the friction function is approximated from the tracer diffusion coefficient as a function of c_M, i.e., the large circles in Figure 6a. As mentioned above, the tracer diffusion coefficient in this experiment describes the friction felt by a probe polymer moving through an environment composed only of the matrix polymer and the solvent. The friction function in eq 9, however, must also account for the finite amount of the probe polymer which must be present to make the measurement of the initial slope. Thus an approximate friction function was constructed from a polynomial representation of $[k_BT/D(c_P \to 0,c_M)]/[k_BT/D(c_P \to 0,0)]$, or $D_0/D_{TR}(c_M)$, with additional terms added to account for the finite concentration of the probe:

$$\frac{f}{f_0} \approx 1.0 + 56.4c_M + 2370c_M^2 + 47900c_M^3 + k_{f,P}c_P + k_{f,PM}c_Pc_M + k_{f,PP}c_P^2 \quad (15)$$

Only second-order terms in c_P have been included since c_P is always relatively low. The concentration range of the probe was constant (with a mean value $\bar{c}_P$ of 0.002 g/mL), so that

$$\frac{f}{f_0} \approx 1.0 + 56.4c_M + 2370c_M^2 + 47900c_M^3 + k' + k''c_M \quad (16)$$

where k' and k'' are given by

$$k' = k_{f,P}c_P + k_{f,PP}c_P^2$$

$$k'' = k_{f,PM}c_P$$

The coefficient k'' describes how the increment of friction contributed by the fixed concentration of polystyrene ($\bar{c}_P$) depends on c_M. Initially, k'' will be taken to be zero and k' will be fixed so as to give the measured value of k_d in the binary solution.

Figure 6b shows the measured values of k_d(app) along with a curve calculated from the measured thermodynamic function and the friction function given in eq 16. A value of approximately 1.0 for k' was required to match the value of k_d in the absence of matrix polymer. Yamakawa[52] has derived an expression relating k_f to the intrinsic viscosity using a random flight model of monodisperse polymer chains:

$$k_f = 1.2A_2M + 0.2[\eta] \quad (17)$$

For polystyrene with molecular weight 1×10^6 in toluene, $A_2 \approx 2.5 \times 10^{-4}$ (mL mol)/g^2, $[\eta] \approx 230$ mL/g, and $k_f \approx 346$ mL/g, and so for $c_P = 0.002$ g/mL, $k_fc_P \approx 0.70$. Thus it appears that the term involving c_P^2 contributes to k' to some extent, even at $c_P/c_P^* \approx 0.25$. From Figure 6b, it is apparent that the calculated k_d(app) values capture the qualitative features quite well and are in fair quantitative agreement with the measured values. To reiterate, the only adjustable parameter to this point is k', which was fixed to give agreement with the value of k_d for $c_M = 0$. Better fits to the measured k_d(app) versus c_M could be obtained by varying k' and k'' simultaneously. However, the value of such a procedure would be questionable, since a completely quantitative test of eq 13 can only be made with an independent measurement of the friction function.

In addition to the pair of probe and matrix polymers discussed above, k_d(app) has also been measured for a PS probe of 2.3×10^5 in the presence of PMMA matrix polymers of 8.4×10^5 and 6.6×10^4. The k_d(app) and $D_{TR}(c_M)$ values as a function of the concentration of both polymers for all three pairs of probe and matrix polymers are given in Table IV. Values of k_d(app) have been calculated for the second and third pairs using eq 13, as described above. The thermodynamic functions for these pairs were not measured, however, but were calculated from the function measured for the first pair, with the assumption that A_2(app)/A_{2o} versus c/c^* is a universal function independent of the molecular weights of the two polymers. Support for this scaling behavior of the thermodynamic function may be obtained from total intensity light scattering from isorefractive ternary solutions,[33,34] as shown earlier.

The measured and calculated values of k_d(app) are compared for all three pairs of probe and matrix polymers in Figure 7. The values of k_d for $c_M = 0$ were subtracted in each case to allow the three sets of data to be clearly displayed on the same plot. One observes that the combination of the thermodynamic and frictional functions according to eq 13 yields the qualitative trends with molecular weight which are observed experimentally. While independent measurements of the thermodynamic and frictional functions for each pair would be necessary for a completely quantitative test, the prediction of the qualitative trends with the probe and matrix molecular weights gives further support to the description of k_d(app) in eq 13. In essence, the thermodynamic influence of the matrix polymer dominates k_d(app) at low matrix concentrations, resulting in the initial decrease, and the friction function, which appears in the denomi-

Table IV
Values of k_d(app) and $D_{TR}(c_M)$ versus Matrix Polymer Concentration for Three Pairs of Probe and Matrix Polymers

poly(methyl methacrylate) concn × 10^3 (g/mL)	k_d(app) (mL/g)	$D_{TR}(c_M)$ (cm²/s)
Polystyrene M_w = 930 000, Poly(methyl methacrylate) M_w = 840 000		
0.000	88.0	1.29×10^{-7}
0.635	45.4	1.30×10^{-7}
1.31	10.0	1.27×10^{-7}
1.73	−4.4	1.25×10^{-7}
2.75	−38.9	1.22×10^{-7}
3.60	−29.6	1.04×10^{-7}
4.77	−45.3	1.02×10^{-7}
6.81	−43.7	8.61×10^{-8}
7.98	−43.6	7.69×10^{-8}
10.8	−42.8	6.39×10^{-8}
12.9	−35.1	5.81×10^{-8}
23.4	−20.7	3.10×10^{-8}
34.8	−10.9	1.65×10^{-8}
Polystyrene M_w = 233 000, Poly(methyl methacrylate) M_w = 840 000		
0.00	39.7	2.65×10^{-7}
0.87	27.1	2.53×10^{-7}
1.36	5.5	2.67×10^{-7}
1.61	−30.9	2.94×10^{-7}
3.47	−53.9	2.70×10^{-7}
5.18	−49.7	2.34×10^{-7}
8.11	−43.4	1.92×10^{-7}
12.4	−38.5	1.87×10^{-7}
26.5	−14.6	7.06×10^{-8}
35.1	−11.2	5.06×10^{-8}
Polystyrene M_w = 233 000, Poly(methyl methacrylate) M_w = 66 000		
0.00	39.6	2.65×10^{-7}
6.67	16.9	2.29×10^{-7}
9.34	0.2	2.23×10^{-7}
19.5	−10.4	1.74×10^{-7}
39.0	−12.3	1.11×10^{-7}
66.8	−9.6	6.15×10^{-8}
80.5	−6.9	4.20×10^{-8}

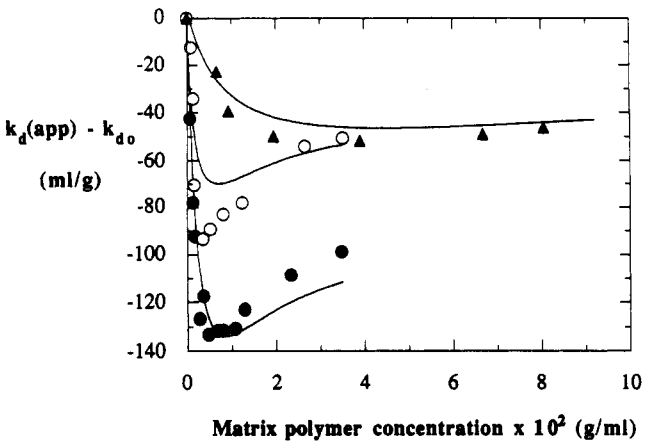

Figure 7. Comparison of measured k_d(app) with curves calculated from eq 13 using experimental estimates of the thermodynamic and friction functions for the following pairs of probe and matrix polymers, respectively: (Δ) 9.3×10^5 and 8.4×10^5; (○) 2.3×10^5 and 8.4×10^5; (●) 2.3×10^5 and 6.6×10^4. The values of k_d in the absence of matrix polymer were subtracted to allow the three sets of data to be clearly displayed on the same plot.

nator of the expression for k_d(app), drives the value of k_d(app) back toward zero at higher concentrations of matrix polymer.

The analysis of k_d(app) presented above has involved the determination of the thermodynamic and frictional functions from experimental data. Comparison of the experimental k_d(app) with theoretical expressions for the two functions is complicated somewhat by the fact that more than lowest order terms must be included to describe the two functions over the experimental concentration ranges. However, general trends may be obtained from expressions which include only lowest order terms. The expression for the thermodynamic function is given to lowest order by

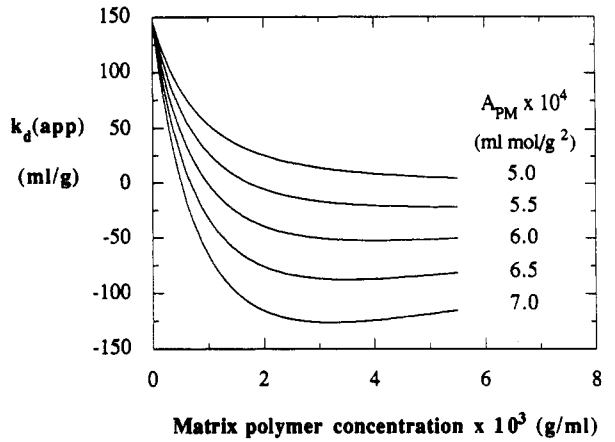

Figure 8. Variation of k_d(app) with A_{PM} evaluated from eq 19 for the case of $M_P = M_M = 1 \times 10^6$, $A_P = A_M$, and $k_{f,P} = k_{f,M}$, where k_f is calculated from eq 17. The parameter values have been set to correspond to PS in toluene and are given in the text.

$$\hat{H}|_{c_P,c_M \to 0} = 1 + 2M_P A_P(\text{app}) c_P \qquad (18)$$

where A_P(app) has been given in eq 1. When this is combined with the lowest order expression for the friction function according to eq 13, the expression for k_d(app) in the limit of $c_P = 0$ is given by

$$k_d(\text{app}) = \frac{2A_P M_P - \dfrac{A_{PM}^2 M_P M_M c_M}{1 + 2A_M M_M c_M}}{1 + k_{f,M} c_M} - \frac{k_{fP}}{(1 + k_{f,M} c_M)^2} \qquad (19)$$

Note that for $c_M = 0$, $k_d = 2A_P M_P - k_{f,P}$, which is the expression for binary solutions. Equation 19 may be used[14] to estimate the effect of the molecular weight of the two polymers, the solvent quality for the two polymers, and the interaction parameter χ_{PM} between the two polymers on k_d(app).

The effect of χ_{PM} is examined by varying the value of the cross virial coefficient A_{PM}, while A_P and A_M are held constant. Figure 8 displays such a comparison for probe and matrix polymers of the same M_w, A_2, and k_f, but which have an unfavorable interaction between them ($\chi_{PM} > 0$). The parameters (except for χ_{PM}) are set to correspond to those for polystyrene with a molecular weight 1×10^6 in toluene. The intrinsic viscosity used in eq 17 for k_f was estimated from[53] $[\eta] = 0.0097M^{0.74}$, determined for polystyrene in toluene at 20 °C. The virial coefficients A_P and A_M are both given the value 2.5×10^{-4} (mL mol)/g². The results are calculated for matrix polymer concentrations up to $c_M = c_M^*$. From Figure 8, it is clear that the depth of the minimum is quite sensitive to the value of A_{PM}. In fact, for this case no minimum occurs unless $A_{PM} > 2A_P = 2A_M$, which may be interpreted as reflecting a positive χ_{PM}. It should be noted that the decrease in k_d(app) occurs even when $\chi_{PM} = 0$ but is enhanced somewhat when the polymers are incompatible ($\chi_{PM} > 0$). In other words, the most important factor affecting k_d(app) is that the environment of the probe chains contains another polymer and the degree of incompatibility between the two polymer types is of secondary importance.

In summary, at low matrix polymer concentrations, k_d(app) is dominated by the thermodynamic influence of the matrix polymer, which causes the rather abrupt decrease in k_d(app). When the solvent is a good solvent for both polymers and $M_P = M_M$, $A_P = A_M$, and $k_{f,P} = k_{f,M}$, a positive χ_{PM} between the two polymers will lead to a minimum in k_d(app), with the frictional influence of the matrix polymer driving the value of k_d(app) back toward zero at higher concentrations. Since toluene is a better solvent for PS than for PMMA, the minima in the experimental curves presented earlier cannot be attributed exclusively to the positive χ_{PM} between the two polymers, although χ_{PM} is expected to influence the depth of the minima. As the molecular weight of the matrix polymer is decreased, the same qualitative features are present but occur at higher concentrations since the thermodynamic term scales roughly as c_M/c_M^*. As the molecular weight of the probe polymer is decreased, the main effect on k_d(app) versus c_M is that k_d in the binary solution decreases due to the decrease in A_2M.

The value of k_d(app) is expected to decrease more rapidly with c_M the poorer the solvent quality toward the matrix polymer. When $A_M = 0$, the numerator of the first term decreases linearly with c_M and the first term reaches a negative plateau value at high c_M. Since the second term approaches zero at high c_M, the value of k_d(app) will not return to zero for this case but will remain at a negative value with magnitude given by $A_{PM}^2 M_P M_M / k_{f,M}$. This prediction may be tested by performing the dynamic light-scattering experiments on solutions in which the solvent is good for the probe, but a θ solvent for the matrix polymer, and for which the solvent has a large refractive index increment for the probe, but is isorefractive with the matrix.

Previously,[54-56] analysis of the initial dependence of the mutual diffusion coefficient on the concentration of probe has been based on the following equations:

$$D = D_{TR}(c_M)(1 + k_d(\text{app})c_P) \tag{20}$$

$$k_d(\text{app}) \cong 2A_2(\text{app})M_P - k_{f,P} \tag{21}$$

$$f(c_M,c_P) = f(0,c_M)(1 + k_{f,P}c_P + ...) \tag{22}$$

which were assumed by analogy with the binary solution expressions. The values of k_d(app) were determined experimentally as the slope of $D_{PP}(c_P,c_M)$ versus c_P divided by the intercept $D_{TR}(c_M)$. This definition of k_d(app)

$$k_d(\text{app}) = \left.\frac{\partial D_{PP}/D_{TR}(c_M)}{\partial c_P}\right|_{c_P=c_P^A} \tag{23}$$

differs from that given in eq 12 in that the constant D_0 has been replaced by $D_{TR}(c_M)$ in the numerator. Substituting eq 9 into eq 23 gives

$$k_d(\text{app}) = \left[\left.\frac{\partial \hat{H}(c_P,c_M)/\partial c_P}{f(c_P,c_M)}\right|_{c_P^A,c_M} - \left.\frac{\hat{H}(c_P,c_M)\dfrac{\partial f(c_P,c_M)}{\partial c_P}}{f(c_P,c_M)^2}\right|_{c_P^A,c_M}\right] f(0,c_M) \tag{24}$$

which differs from eq 13 in that the $f(0,c_M)$ has replaced the constant f_0. The term in square brackets describes the change in the slopes of the lines in Figure 6a. Thus the definition of k_d(app) given in eq 23 corresponds to the ratio of two functions: the function shown in Figure 6b, which describes the change in the slopes of the lines in Figure 6a, and the function which describes the decrease in the tracer diffusion coefficient, which is given by the solid curve through the large circles in Figure 6a. The definition of k_d(app) in eq 12, on the other hand, describes only the change in the slopes of the lines in Figure 6a. While both definitions are valid, the definition in eq 12 may give more direct insight into the competition between the thermodynamic and frictional effects.

In the limit of $c_P \to 0$, eq 21 follows from eq 24 when eqs 1 and 22 are inserted for the thermodynamic and friction functions. Equation 21 may be somewhat misleading, in that the second term appears to be independent of c_M. This is due to the form of the friction function in eq 22. If the friction function is expressed as

$$f(c_P,c_M) = f_0(1 + k_{f,P}c_P + k_{f,M}c_M + ...) \tag{25}$$

then k_d(app) according to the definition in eq 23 is given by

$$k_d(\text{app}) = 2A_2(\text{app})M_P - \frac{k_{f,P}}{(1 + k_{f,M}c_M)} \tag{26}$$

The concentration dependence appearing in the second term is important in interpreting the thermodynamic and frictional contributions to k_d(app). From eqs 26 and 19, both terms decrease with increasing c_M in either definition of k_d(app). When the two terms are plotted versus c_M,[14] it is apparent that in either definition both terms may contribute to k_d(app) even when the matrix polymer is semidilute. For example, using the thermodynamic and frictional functions (estimated from experimental data) which were shown to describe the data in Figure 6b, the contributions of the two terms in eq 26 are roughly equal at $c_M \cong 3c_M^*$. Therefore, it seems that inferences drawn[56] by direct analogy with the binary solution expression, assuming that only the thermodynamic term is present when the matrix polymer is semidilute, may be premature.

Summary

From total intensity and dynamic light-scattering experiments, the most significant influence of the matrix polymer on a probe in dilute solution is to alter the thermodynamic environment of the probe. The fact that the environment for the probe contains another polymer leads to a decrease in the apparent second virial coefficient of the probe with increasing matrix polymer concentration. When the molecular weights of the probe and matrix polymers are similar, the probe begins to sense the matrix polymer at matrix polymer concentrations about 1 order of magnitude below c_M^*, as seen in Figure 2c. The decrease in the apparent second virial coefficient apparently reflects the volume excluded from the probe by the matrix polymers, since the decrease in A_M(app) scales approximately with c_M/c_M^*. For probe and matrix polymers with similar molecular weights, there is little increase in the friction (or decrease in D_{TR}) experienced by the probe below c_M^* and negligible decrease in probe coil size below c_M^*, so the thermodynamic influence of the matrix polymer appears to be the dominant effect.

The dynamic manifestation of the thermodynamic effect is a decrease in the rate of dissipation of fluctuations in the concentration of the probe, or D_{PP}. This has not been widely recognized before, although a few studies have been reported.[54-56] A ramification of this is discussed in a forthcoming paper[57] regarding the rates of chemical reactions between macromolecules. If the dynamic light-

scattering experiments are conducted for low matrix polymer concentrations, and if the range of probe concentration is as low as possible, it may be possible to extract the osmotic cross virial coefficient A_{PM} from the dynamic experiment. However, this requires prior knowledge of A_P, A_M, and $f(c_P,c_M)$. Possible advantages for extracting A_{PM} from the dynamic experiment rather than from the total intensity experiment are that the dynamic experiment may give greater accuracy and that the minimum in k_d(app) vs C_M may give greater sensitivity to A_{PM}. The principal value of the dynamic experiment, however, is that it gives insight into the competition between the thermodynamic and frictional effects of the matrix polymer.

Both the viscosity and total intensity light-scattering experiments show that no additional effects can be attributed to the positive χ_{PM} for this system. The value of the Huggins coefficient describing the cross interaction in a mixture is in the same range as the values for the two polymers in binary solutions. Both experiments indicate that there is no contraction of the probe coil below c^*, when matrix and probe polymers have similar molecular weights. Above c^*, contraction of the probe coil with matrix polymer concentration is similar to the behavior observed in binary solutions by small-angle neutron scattering. However, analysis of the lowest order expression for k_d(app) shows that the minimum in k_d(app) versus c_M can be quite sensitive to the value of A_{PM}. In the present system, though, it is difficult to assess the role of χ_{PM} quantitatively from the minima of the k_d(app) versus c_M curves, since the solvent quality is significantly different for the two polymers and more than lowest order terms are required to describe the data over the experimental concentration range. It should be noted that a decrease in k_d(app) still occurs when $\chi_{PM} = 0$, but that the effect of $\chi_{PM} > 0$ is to produce a somewhat more dramatic decrease.

Comparison of the contraction of the radius of gyration of a probe polymer as a function of matrix concentration for three matrix polymers varying widely in molecular weight gives insight into the molecular weight ratio for which the smaller matrix chains penetrate the domain of the larger probe coil in dilute solution. It appears that the transition between the two limits of noninterpenetrating ($M_P = M_M$, $c < c^*$) and interpenetrating ($M_P \gg M_M$, $c_M < c_M^*$) may be characterized by a rather abrupt transition occurring over a limited range of M_P/M_M, rather than by a continuous transition with increasing M_P/M_M.

Acknowledgment. The support of the National Science Foundation, through Grant DMR-8715391 to T.P.L., is gratefully acknowledged. M.T. acknowledges with thanks the support of the Shell Companies Foundation. We acknowledge with appreciation the support of the Center for Interfacial Engineering, an NSF-supported Engineering Research Center.

Appendix

The flux expressions for a ternary polymer–polymer–solvent system can be written in general as

$$J_P = -(L_{PP}\alpha_{PP} + L_{PM}\alpha_{MP})\nabla\mu_P - (L_{PP}\alpha_{PM} + L_{PM}\alpha_{MM})\nabla\mu_M \quad (A.1)$$

$$J_M = -(L_{PM}\alpha_{PP} + L_{MM}\alpha_{MP})\nabla\mu_P - (L_{PM}\alpha_{PM} + L_{MM}\alpha_{MM})\nabla\mu_M \quad (A.2)$$

where

$$\alpha_{ij} = (\delta_{ij} + c_j V_i/c_S V_S) \quad \text{and} \quad c_S V_S + c_P V_P + c_M V_M = 1$$

and i and j refer to the two polymers, the subscripts S, P, and M refer to the solvent, probe polymer, and matrix polymer, respectively, J_i are the fluxes relative to the volume average velocity, L_{ij} are the Onsager coefficients, μ_i are the chemical potentials per unit mass of the two polymers, and V_i are the partial specific volumes. Since

$$\nabla\mu_P = \frac{\partial\mu_P}{\partial c_P}\nabla c_P + \frac{\partial\mu_P}{\partial c_M}\nabla c_M \text{ and } \nabla\mu_M = \frac{\partial\mu_M}{\partial c_P}\nabla c_P + \frac{\partial\mu_M}{\partial c_M}\nabla c_M$$

then

$$D_{PP} = L_{PP}\left(\alpha_{PP}\frac{\partial\mu_P}{\partial c_P} + \alpha_{PM}\frac{\partial\mu_M}{\partial c_P}\right) + L_{PM}\left(\alpha_{MP}\frac{\partial\mu_P}{\partial c_P} + \alpha_{MM}\frac{\partial\mu_M}{\partial c_P}\right) \quad (A.3)$$

$$D_{PM} = L_{PP}\left(\alpha_{PP}\frac{\partial\mu_P}{\partial c_M} + \alpha_{PM}\frac{\partial\mu_M}{\partial c_M}\right) + L_{PM}\left(\alpha_{MP}\frac{\partial\mu_P}{\partial c_M} + \alpha_{MM}\frac{\partial\mu_M}{\partial c_M}\right) \quad (A.4)$$

where D_{PP} and D_{PM} are defined by $J_P = -D_{PP}\nabla c_P - D_{PM}\nabla c_M$. Assuming that $D_{PM} \to 0$ for solutions which are relatively dilute in both polymeric components, then

$$D_{PP} = L_{PP}(\alpha_{PP}\alpha_{MM} - \alpha_{PM}\alpha_{MP}) \times \frac{\left(\frac{\partial\mu_P}{\partial c_P}\right)\left(\frac{\partial\mu_M}{\partial c_M}\right) - \left(\frac{\partial\mu_M}{\partial c_P}\right)\left(\frac{\partial\mu_M}{\partial c_P}\right)}{\alpha_{MP}\frac{\partial\mu_P}{\partial c_M} + \alpha_{MM}\frac{\partial\mu_M}{\partial c_M}} \quad (A.5)$$

The Onsager coefficient L_{PP} may be written as

$$L_{PP} = \frac{c_P M_P}{N_A f(c_P,c_M)} \quad (A.6)$$

which is a generalization of the binary solution expression[51] in that the friction felt by the probe polymer moving through the ternary solution $f(c_P,c_M)$ is a function of both probe and matrix polymer concentrations. Thus the mutual diffusion coefficient is given by

$$D_{PP} = \frac{c_P M_P}{N_A f(c_P,c_M)} \times \frac{\left(\frac{\partial\mu_P}{\partial c_P}\right)\left(\frac{\partial\mu_M}{\partial c_M}\right) - \left(\frac{\partial\mu_P}{\partial c_M}\right)\left(\frac{\partial\mu_M}{\partial c_P}\right)}{c_M V_P\left(\frac{\partial\mu_P}{\partial c_M}\right) + (c_S V_S + c_M V_M)\left(\frac{\partial\mu_M}{\partial c_M}\right)} \quad (A.7)$$

Note that for $c_M = 0$

$$D_{PP} = \frac{c_P M_P}{N_A f(c_P) c_S V_S}\frac{\partial\mu_P}{\partial c_P} \quad (A.8)$$

which is the well-known[43-48,51] result for the mutual diffusion coefficient in binary solutions. For $c_P \to 0$

$$c_S V_S = 1 - c_P V_P, \quad \frac{\partial\mu_P}{\partial c_P} = \frac{RT}{M_P}\left(\frac{1}{c_P} + 2A_P M_P + \ldots\right),$$

and $f(c_P) = f_0(1 + k_f c_P + \ldots)$

so

$$D_{PP} = \frac{k_B T}{f_0}(1 + c_P V_P + ...)(1 - k_f c_P + ...)(1 + 2A_P M_P c_P + ...)$$
$$= \frac{k_B T}{f_0}(1 + k_d c_P + ...) \quad (A.9)$$

where k_B is Boltzmann's constant, T is the temperature, and the $k_d = 2A_P M_P - k_f + V_P$.

For ternary solutions which are dilute in both polymeric components, it follows from eq A.7 that

$$D_{PP} \approx \frac{k_B T}{f(c_P,c_M)} c_P M_M \left[\frac{\left(\frac{\partial \mu_P}{\partial c_P}\right)\left(\frac{\partial \mu_M}{\partial c_M}\right) - \left(\frac{\partial \mu_P}{\partial c_M}\right)\left(\frac{\partial \mu_M}{\partial c_P}\right)}{\frac{\partial \mu_M}{\partial c_M}} \right] \quad (A.10)$$

or

$$D_{PP} = \frac{k_B T}{f_0} \frac{\hat{H}(c_P,c_M)}{\hat{f}(c_P,c_M)} \quad (A.11)$$

where

$$\hat{H}(c_P,c_M) = \frac{c_P M_P}{RT} \left[\frac{\left(\frac{\partial \mu_P}{\partial c_P}\right)\left(\frac{\partial \mu_M}{\partial c_M}\right) - \left(\frac{\partial \mu_P}{\partial c_M}\right)\left(\frac{\partial \mu_M}{\partial c_P}\right)}{\frac{\partial \mu_M}{\partial c_M}} \right] \quad (A.12)$$

and

$$\hat{f}(c_P,c_M) = \frac{f(c_P,c_M)}{f_0} \quad (A.13)$$

Equation A.10 shows that the mutual diffusion coefficient measured by dynamic light scattering from isorefractive ternary solutions can be written as a thermodynamic driving force divided by a frictional resistance, just as in binary solutions. In ternary solutions, however, both factors are functions of the concentrations of both polymers. An alternative derivation of eq A.10 has recently been reported by Aven and Cohen.[56]

The dimensionless function in eq A.12 is the same function which appears in the description of the total intensity of light scattered by the isorefractive ternary solution. It can be shown that for $\nu_M = 0$[12]

$$\frac{Kc_P}{R_{\theta=0}} = \frac{c_P}{RT} \left[\frac{\left(\frac{\partial \mu_P}{\partial c_P}\right)\left(\frac{\partial \mu_M}{\partial c_M}\right) - \left(\frac{\partial \mu_P}{\partial c_M}\right)\left(\frac{\partial \mu_M}{\partial c_P}\right)}{\frac{\partial \mu_M}{\partial c_M}} \right] \quad (A.14)$$

The value of this function at $c_P = 0$ is the inverse of the weight average molecular weight of the probe, so that for a monodisperse probe polymer

$$\frac{\frac{Kc_P}{R_{\theta=0}}}{\frac{Kc_P}{R_{\theta=0}}\Big|_{c_P=0}} = \frac{c_P M_P}{RT} \left[\frac{\left(\frac{\partial \mu_P}{\partial c_P}\right)\left(\frac{\partial \mu_M}{\partial c_M}\right) - \left(\frac{\partial \mu_P}{\partial c_M}\right)\left(\frac{\partial \mu_M}{\partial c_P}\right)}{\frac{\partial \mu_M}{\partial c_M}} \right] \quad (A.15)$$

Thus, the thermodynamic function may be easily obtained by total intensity light scattering.

It is also possible to measure the frictional function in eq A.10 independently. Forced Rayleigh scattering,[58] for example, may be used to measure the tracer diffusion coefficient of a dye-labeled polymer as a function of the composition of the solution. The tracer diffusion coefficient is given by the Einstein equation:

$$D_{TR} = \frac{k_B T}{f(c)} \quad (A.16)$$

where c is the total concentration of polymer. If the dye-labeled polymer is of the same type and molecular weight as the probe polymer and the composition of the solution is the same as in the dynamic light-scattering experiments, then the friction function obtained from $k_B T/D_{TR}$ should be the same as that appearing in eq A.10.

References and Notes

(1) Fukuda, T.; Nagata, M.; Inagaki, H. *Macromolecules* **1984**, *17*, 548.
(2) Fukuda, T.; Nagata, M.; Inagaki, H. *Macromolecules* **1986**, *19*, 1411.
(3) Fukuda, T.; Nagata, M.; Inagaki, H. *Macromolecules* **1987**, *20*, 654.
(4) Fukuda, T.; Nagata, M.; Inagaki, H. *Macromolecules* **1987**, *20*, 2173.
(5) Hyde, A. J.; Tanner, A. G. *J. Colloid Interface Sci.* **1968**, *28*, 179.
(6) Kaddour, L. O.; Strazielle, C. *Polymer* **1987**, *28*, 459.
(7) Kaddour, L. O.; Strazielle, C. *Eur. Polym. J.* **1988**, *24*, 117.
(8) Vrij, A.; van den Esker, M.; *J. Polym. Sci., Polym. Phys. Ed.* **1975**, *13*, 727.
(9) Van den Esker, M.; Laven, J.; Broeckman, A.; Vrij, A. *J. Polym. Sci., Polym. Phys. Ed.* **1976**, *14*, 1953.
(10) Kratochvil, P.; Vorlicek, J.; Strakova, D.; Tuzar, Z. *J. Polym. Sci., Polym. Phys. Ed.* **1975**, *13*, 2321.
(11) Kratochvil, P.; Vorlicek, J. *J. Polym. Sci., Polym. Phys. Ed.* **1976**, *14*, 1561.
(12) Kent, M. S.; Tirrell, M.; Lodge, T. P. *Polymer* **1991**, *32*, 314.
(13) Balloge, S.; Tirrell, M. *Macromolecules* **1985**, *18*, 817–819.
(14) Kent, M. S. Ph.D. Thesis, University of Minnesota, 1990.
(15) Koppel, D. E. *J. Chem. Phys.* **1972**, *57*, 4814.
(16) Bargeron, C. B. *J. Chem. Phys.* **1974**, *60*, 2516.
(17) Bargeron, C. B. *J. Chem. Phys.* **1974**, *61*, 2134.
(18) Benmouna, M.; Benoit, H.; Duval, M.; Akcasu, Z. *Macromolecules* **1987**, *20*, 1107.
(19) Foley, G.; Cohen, C. *Macromolecules* **1987**, *20*, 1891.
(20) Provencher, S. W.; Hendrix, J.; De Maeyer, L.; Paulussen, N. *J. Chem. Phys.* **1978**, *69*, 4273.
(21) Standard Specifications and Operating Instructions for Glass Capillary Kinematic Viscometers. *Annual Book of ASTM Standards*; ASTM: Philadelphia, 1987, D446-85a, Vol. 5.01, p 243.
(22) Standard Test Method for Dilute Solution Viscosity of Polymers. *Annual Book of ASTM Standards*; ASTM: Philadelphia, 1987; D2857-70, Vol. 8.02, p 620.
(23) Daoud, M.; Cotton, J. P.; Farnoux, B.; Jannink, G.; Sarma, G.; Benoit, H.; Duplessix, R.; Picot, C.; de Gennes, P. G. *Macromolecules* **1975**, *8*, 804.
(24) de Gennes, P. G. *Scaling Concepts in Polymer Physics*; Cornell University Press: Ithaca, NY, 1979.
(25) Brochard, F. *J. Phys. (Paris)* **1981**, *42*, 505.
(26) de Gennes, P. G. *J. Polym. Sci. C, Polym. Symp* **1977**, *61*, 313.
(27) Joanny, J. F.; Grant, P.; Turkevich, L. A.; Pincus, P. *J. Appl. Phys.* **1981**, *52*, 5943.
(28) Joanny, J. F.; Grant, P.; Turkevich, L. A.; Pincus, P. *J. Phys. (Paris)* **1981**, *42*, 1045.
(29) Nose, T. *J. Phys. (Paris)* **1986**, *47*, 517.
(30) Momii, T.; Numasawa, N.; Kuwamoto, K.; Nose, T. *Macromolecules* **1991**, *24*, 3964.
(31) Baba, J.; Kubo, T.; Takano, A.; Nose, T. *Polym. Prepr., Jpn. (Engl. Ed.)* **1991**, *40*, E1644.
(32) Cotts, D. R. *J. Polym. Sci., Polym. Phys. Ed.* **1983**, *21*, 1381.
(33) Lin, C. Y.; Rosen, S. L. *J. Polym. Sci., Polym. Phys. Ed.* **1982**, *20*, 1497.
(34) Kuhn, R.; Cantow, H. J. *Makromol. Chem.* **1969**, *122*, 65.
(35) Numasawa, N.; Hamada, T.; Nose, T. *J. Polym. Sci., Lett. Ed.* **1985**, *23*, 1.
(36) Numasawa, N.; Kuwamoto, K.; Nose, T. *Macromolecules* **1986**, *19*, 2593.
(37) Lodge, T. P.; Markland, P.; Wheeler, L. M. *Macromolecules* **1989**, *22*, 3409.
(38) Cantow, H. J.; Schulz, G. V. *Z. Phys. Chem. (Munich)* **1954**, *30*, 365.

(39) Flory, P. J. *J. Chem. Phys.* **1949**, *17*, 303.
(40) Kirste, R.; Lehnen, B. *Makromol. Chem.* **1976**, *177*, 1137.
(41) Kirkwood, J. G.; Goldberg, R. J. *J. Chem. Phys.* **1950**, *18*, 54. Stockmayer, W. H. *J. Chem. Phys.* **1950**, *18*, 58.
(42) Kotaka, T.; Tanaka, T.; Ohnuma, H.; Murakami, Y.; Inagaki, H. *Polym. J.* **1970**, *1*, 245.
(43) Moszkowicz, M. J.; Rosen, S. L. *J. Polym. Sci., Polym. Phys. Ed.* **1979**, *17*, 715.
(44) Hanley, B. F. Ph.D. Thesis, University of Minnesota, 1987.
(45) Mandema, W.; Zeldenrust, H. *Polymer* **1977**, *18*, 835.
(46) Han, C. C. *Polymer* **1979**, *20*, 259.
(47) Roots, J.; Nystrom, B.; Sundelof, L.-O.; Porsch, B. *Polymer* **1979**, *20*, 337.
(48) Akcasu, A. Z. *Polymer* **1981**, *22*, 1169.
(49) Han, C. C.; Akcasu, A. Z. *Polymer* **1981**, *22*, 1165.
(50) Venkataswamy, K.; Jamieson, A. M. *Macromolecules* **1986**, *19*, 124.
(51) de Gennes, P. G. *J. Chem. Phys.* **1971**, *55*, 572.
(52) Yamakawa, H. *Modern Theory of Polymer Solutions*; Harper and Row Publishers, Inc.: New York, 1971.
(53) Ewart, R. H.; Tingey, H. C. *Abstracts of Papers*, 111th National Meeting of the American Chemical Society, Atlantic City, NJ, April 1947; American Chemical Society: Washington, DC, 1947.
(54) Wheeler, L. M.; Lodge, T. P.; Hanley, B. F.; Tirrell, M. *Macromolecules* **1987**, *20*, 1120.
(55) Chang, T.; Han, C. C.; Wheeler, L. M.; Lodge, T. P. *Macromolecules* **1988**, *21*, 1870.
(56) Aven, M. R.; Cohen, C. *Macromolecules* **1990**, *23*, 476.
(57) Kent, M. S.; Faldi, A.; Tirrell, M.; Lodge, T. P. *Macromolecules* **1992**, *25*, 4501.
(58) Leger, L.; Hervet, H.; Rondelez, F. *Macromolecules* **1981**, *14*, 1732.

Registry No. PS (homopolymer), 9003-53-6; PMMA (homopolymer), 9011-14-7; $C_6H_5CH_3$, 108-88-3; PhC(O)OEt, 93-89-0.